Saudi Pharmaceutical Journal 31 (2023) 101785

HOSTED BY

Contents lists available at ScienceDirect

Saudi Pharmaceutical Journal

journal homepage: www.sciencedirect.com

Original article

# In-vitro and ex-vivo antidiabetic, and antioxidant activities of Box-Behnken design optimized *Solanum xanthocarpum* extract loaded niosomes

Rama Tyagi [a], Ayesha Waheed [b], Neeraj Kumar [b], Mohd. Mujeeb [c], Tanveer Naved [a], Mohammad Rashid Khan [d], Khaled Alhosaini [d], Yasser A. Alqarni [d], Rani Rahat [e], Perwez Alam [f,*], Swati Madan [a,*]

[a] Amity Institute of Pharmacy, Amity University, Noida, Uttar Pradesh 201301, India
[b] Department of Pharmaceutics, SPER, Jamia Hamdard, New Delhi 110062, India
[c] Department of Pharmacognosy and Phytochemistry, SPER, Jamia Hamdard, New Delhi 110062, India
[d] Department of Pharmacology and Toxicology, College of Pharmacy, King Saud University, P.O. Box 2457, Riyadh 11451, Saudi Arabia
[e] Department of Periodontics, College of Dentistry, University of Illinois Chicago, Chicago, IL 60612, USA
[f] Department of Pharmacognosy, College of Pharmacy, King Saud University, P.O. Box 2457, Riyadh 11451, Saudi Arabia

ARTICLE INFO

*Article history:*
Received 5 June 2023
Accepted 8 September 2023
Available online 14 September 2023

*Keywords:*
Nanoformulation
Diabetes
Niosome
CLSM
Box-behnken design

ABSTRACT

One of the most prevalent lifestyle diseases, diabetes mellitus (DM) is brought on by an endocrine issue. DM is frequently accompanied by hyperglycemia, a disease that typically results in an excess of free radicals that stress tissues. The medical community is currently concentrating on creating therapeutic medications with roots in nature to lessen the damage associated with hyperglycemia. *Solanum xanthocarpum* has a number of medicinal benefits. The investigation aimed to produce and analyze niosomal formulations containing *S. xanthocarpum* extract (SXE). Niosomes were made by implementing the solvent evaporation process, which was further optimized using Box-Behnken design. Drug release, DPPH assessments, α-amylase inhibition assay, α-glucosidase inhibition assay, and confocal laser scanning microscopy (CLSM) investigation were all performed on the developed formulation (SXE-Ns-Opt). SXE-Ns-Opt displayed a 253.6 nm vesicle size, a PDI of 0.108, 62.4% entrapment efficiency, and 84.01% drug release in 24 h. The rat's intestinal CLSM image indicated that the rhodamine red B-loaded SXE-Ns-Opts had more intestinal penetration than the control. Additionally, the antioxidant effect of the obtained formulation was demonstrated as 89.46% as compared to SXE (78.10%). Additionally, acarbose, SXE, and SXE-Ns-Opt each inhibited the activity of α-amylase by 95.11%, 85.88%, and 89.87%, and also suppressed the enzyme of α-glucosidase by 88.47%, 81.07%, and 85.78%, respectively. To summarise, the establishment of the SXE-Ns-Opt formulation and its characterization demonstrated the legitimacy of the foundation. A promising candidate for the treatment of diabetes mellitus has been shown as *in vitro* studies, antioxidant against oxidative stress, CLSM of rat's intestine and a high degree of penetration of formulation.



## 1. Introduction

Type 2 diabetes is one of the metabolic illness, serious threat and major global health issue. This pathology has direct or indirect detrimental effect on the quality of life as it is linked to the increasing insulin resistance or impairing insulin secretion. There are a variety of antidiabetic drugs used to control or treat type2diabetes. However, most of them are ineffective because of resistance and many unwanted side effects (Padhi et al., 2020). Diabetes and obesity are two major metabolic illnesses that have a negative impact

* Corresponding authors at: Amity Institute of Pharmacy, Amity University, Noida, India (S. Madan). Department of Pharmacognosy, College of Pharmacy, King Saud University, Riyadh, Kingdom of Saudi Arabia (P. Alam).
*E-mail addresses:* aperwez@ksu.edu.sa (P. Alam), smadan3@amity.edu (S. Madan), smadan3@amity.edu (S. Madan).

Peer review under responsibility of King Saud University.

Production and hosting by Elsevier

https://doi.org/10.1016/j.jsps.2023.101785
1319-0164/

on individual's life and are the main reasons for the loss of life in developed nations. Globally, the chronicity of diabetes has risen from 108 million in 1980 to 463 million in 2019, with 1.6 million fatalities attributable to it in 2016. It is predicted that this number would climb to 643 million by 2030 and 783 million by 2045 (https://www.diabetesatlas.org/) (Gudise et al., 2021). As per the World Health Organization, nearly 80% population of the world uses herbal therapies to treat various diseases, garnering increasing interest in discussions about global healthcare. Therefore, the development of low toxicity and high efficiency antidiabetic drugs with good cost-effectiveness ratio is still needed.

Herbs, plants and their active phytoceuticals as flavonoids, terpenopids polyphenols, alkaloids glycosides and essential oils have been documented since ancient times. As various phytoceuticals and plant extracts are responsible for different therapeutic actions but many issues which renders in achieving targeted therapeutic effects are as storage for long duration, degradation/inactivation during transportation, their solubility, size of phytoceuticals (for permeation), temperature, moisture, pH, targeted site, stability, changes in physical, chemical and biological properties, patients' acceptance with medication, persistence, convenient way of administration, and many more (Jeevanandam et al., 2016; Wickramasinghe et al., 2022). Another predicaments and challenges related to pharmacokinetics for phytoceuticals and plant extracts has been as their down regulation and degradation by acids and enzymes in the GIT, bioavailability and metabolism by liver (Hsueh et al., 2017). Development of drug delivery carriers for targeted, controlled and sustained release is essential and further characterized by overcoming the issues by accelerating the bioavailability and biocompatibility of the herbal drugs fitted into carriers. To cure the low solubility and low bioavailability curcumin and tetrandrine were encapsulated into liposome (Song et al., 2022). Taxifolin is an anticancer and antiproliferative effects but limitations that are rendering its clinical applications are water insolubility and size of molecule that prevents its penetration into the biological membrane (Wang et al., 2020). To conquer these difficulties, taxifolin was incorporated into phytosomes which increase the lipophilicity and so enhance the bioavailability into the membrane (Kumar et al., 2021). *G. biloba* when administered orally shows low bioavailability and a short half-life. Incorporation of *G. biloba* into niosomes provided protection from enzymatic degradation, increased entrapment efficiency and duration of stability (Jin et al., 2013).

*Solanum xanthocarpum* Schrad. & Wendl. (Family: Solanaceae) commonly called as Indians nightshade, growing perennial herb, very prickly, diffuses bright green perennial weed with bright green leaves, woody at the base and zigzag stem. Various therapeutic activities admissible to conventional treatment or cure have been mentioned as immunomodulatory, anthelmintic, antipyretic, laxative, antioxidant, antifungal, antibacterial, anti-asthamatic, antimalarial, Wound healing, antidiabetic, hepatoprotective, antiulcer, cardio-protective, anti-hyperlipedemic activity, antifertility activity (Joghee, 2019; Poongothai et al., 2011; Sachin Parmar, Amit Gangwal, 2011). The fruit extract of *S. xanthocarpum* was used to synthesize silver nanoparticles and exhibited antimicrobial activity against MDR clinically isolated Gram-negative. Synthesized silver nanoparticles also tested against the strains of Helicobacter pylori. Nanoparticles showed potent activity against antibiotic resistance and significant inhibition of *H. pylori* urease enzyme (Pungle et al., 2023). Gold nanoparticles were also evaluated for the anticancer activity which showed the suppression of viability and colony formation of NPC cells (C666-1) (Zhang et al., 2018).

This study was design to prepare and characterize the optimized *S. xanthocarpum* extract (SXE)-niosomes using Box-Behnken Design. The optimized formulation was used to explore the *in-vitro* and *in-vivo* therapeutic effect on diabetes, and antioxidant study.

## 2. Materials and methods

### 2.1. Materials

"Span 20, Disodium hydrogen phosphate, cholesterol and potassium dihydrogen phosphate were procured from SD Fine chemicals, Mumbai, India". α-amylase and α-glucosidase (Sigma-Aldrich, Merck, Mumbai), Sulphuric acid, HCl, methanol and ethanol (LR grade and AR grade) purchased from Merck, Mumbai, India.

### 2.2. Methods

#### 2.2.1. Extraction preparation of S. xanthocarpum

Whole plant of *S. xanthocarpum* was congregated from Khari Baoli, New Delhi, India. Dr. Sunita Garg (NISCAIR, New Delhi) confirmed and identified *S. xanthocarpum* and its voucher specimen with code NISCAIR/RHMD/Consult/2020/3656–57-1 was deposited at herbarium for future references. The Whole plant of *S. xanthocarpum* was cleaned, washed and dried in the shade. Dried powder of sample was prepared and then 50 g of powder was extracted with ethanol using Soxhlet for 72 h and filtered. The extract was filtered and evaporated under reduced pressure at 65 °C in a rotary evaporator and stored under 20 °C until needed for further study (Ahn et al., 2020).

#### 2.2.2. Measurement of total phenolic content (TPC) and total flavonoid content (TFC)

To demonstrate the total phenolic content, 2 mL of Folin–Ciocalteu's reagent was added to the prepared extract of various concentrations (50–500 μg/mL). After incubation for 30 min, 2.5 mL of 15% sodium carbonate solution was added to reaction mixture, and the reaction mixture was incubated for 90 min in the dark. The blank sample was prepared without reaction mixture. The absorbance by spectrophotometer (760 nm) was measured and Gallic acid was chosen as a reference. A calibration curve was prepared and the results were expressed as milligram of Gallic acid equivalents/gram. All samples were analyzed in triplicate. The $AlCl_3$colorimetricassaywas considered examining the total flavonoid content (TFC). Each sample of extract was mixed with 5% $NaNO_2$ and 2 mL quantity of distilled water. 10% $AlCl_3$ was combined with the aforementioned reaction mixture and let to sit at room temperature for 15 min. Quercetin was used as a standard solution and absorbance was measured at 430 nm. The TFC was expressed as milligram of quercetin equivalents/gram. All samples were analyzed in triplicate (Gedikoğlu et al., 2019).

#### 2.2.3. Preparation of niosomes loaded with S. xanthocarpum extract

The preparation of *S. xanthocarpum* loaded niosomes (SXE-Ns) was done by significant modifications (Cetin et al., 2022). For the preparation of niosomes, materials used were Span 20, cholesterol and *S. xanthocarpum* extract. *S. xanthocarpum* extract was dissolved in ethanol, along with Span 20 and cholesterol. The aqueous phase (Milli-Q water) was kept on a magnetic stirrer with 1000 rpm at 75 °C and resulting ethanolic phase was added drop by drop. After achieving complete addition of ethanolic phase to aqueous phase, the stirring was mandatory until complete vaporation of ethanol. Lastly, the mixture was sonicated to obtain niosomes vesicles from the prepared niosomes formulation.

*2.2.4. Optimization of SXE loaded niosomes*

Design expert software 11, Stat-Ease, MN, USA) was employed to optimize and prepared SXE-Ns, designing 3-factor, 3-level Box-Behnken design. Cholesterol, Span 20, and sonication time were mentioned as independent variables with their high and low levels. Vesicles size, PDI and %EE were considered as the dependent variables. A total of 15 formulations were prepared and are mentioned in Table 1. The polynomial equation and response surface plots were applied to show the impact of independent variables. The polynomial equation was also used to estimate the impact of different models such as linear and quadratic on the dependent variables via the independent variables.

*2.2.5. Vesicles size and PDI analysis*

The developed SXE-Ns were investigated for vesicle size and PDI by using dynamic light scattering, a Zeta sizer (Malvern Instruments, Worcestershire, UK). The investigation was processed with samples (up to 50 times) using Mili-Q water and temperature regulated at 25 ± 1 °C and at an angle of 90° (Raafat and El-Zahaby, 2020).

*2.2.6. Estimation of entrapment efficiency percent (EE%)*

The EE% of SXE-Ns was analyzed by a separation technique (ultracentrifugation)(Yang, 2019). API loaded *S. xanthocarpum* extract sample was transferred into centrifuge tube at 2000 rpm for 30 min at 4 °C (Remi CPR-24 centrifuge). The clear superior layer was collected and analyzed for the unentrapped drug content. The percentage was determined by using the following formula:

$$\%EE = Dt - Ds/Dt \times 100$$

Where, Dt is the total amount of SXE in niosomes and Ds is the amount of SXE in the supernatant.

*2.2.7. Morphological analysis*

For evaluation of the morphological attributes, SXE-Ns sample was investigated by transmission electron microscopy (JEOL 120CX Microscope, Japan). The sample was further diluted to semi-transparent so that the beam of electrons can pass through the sample easily. The dispersion was placed on the carbon-coated copper grid and enclosed with a film of carbon to adhere to the carbon substrate. Further, to visualize the morphology under TEM, 1% phosphotungstic acid was placed and provide a negative charge on niosomes (Pradeepa et al., 2017).

*2.2.8. Thermal analysis*

The entrapment and nature of drug was confirmed by DSC (Perkin Elmer, Pyris 6 DSC, USA). The DSC was performed for cholesterol, span 20, pure drug and lyophilized SXE-Ns. An aluminum pan was used to place a small amount sample in it and then sealed the pan. The range of temperature was measured from 40 °C to 400 °C. For lyophilization, mannitol with cryoprotectant property was into formulation before placing in freeze dryer (Ghasemian et al., 2017).

**Table 1**
Independent variables used to prepare and optimize SXE-Ns by Box–Behnken design.

| Variables | Low | High |
|---|---|---|
| Independent variables | | |
| X1 = Cholesterol (mg) | 80 | 120 |
| X2 = Span 20 (mg) | 60 | 80 |
| X3 = Sonication time (min) | 2 | 3 |
| Dependent variables | | |
| Y1 = Vesicles size(nm) | | |
| Y2 = PDI | | |
| Y3 = Entrapment (%) | | |

*2.2.9. FTIR analysis*

Fourier transformation infrared spectroscopy (FTIR) scanning was implemented for the sample SXE, SXE-Ns-Opt within the range from 4000 to 400 $cm^{-1}$ employing KBr disc method by Bruker spectrometer (Vertex 70 FTIR-FT Raman) (Abdel-Moneim et al., 2020). For the concoction of pellets, the KBr was triturated and combined with samples and compressed at a 27 pressure of 6 ton/ $cm^2$ using a Shimadzu SSP-CoA IR compression machine (Rani et al., 2017).

*2.2.10. Assessment of in-vitro drug release study*

The dialysis technique was implemented to examine the *in-vitro* release of SXE-Ns-Opt samples among which 1 mL of SXE-Ns-opt was retained in the dialysis bag (Bari et al., 2015). Sample retained in the dialysis bag was processed further by placing it in a beaker containing phosphate buffer solution of pH 7.4 (PBS) at 37 °C and stirred using a magnetic stirrer at 100 rpm. A conventional time conditioned procurement of sample aliquots was performed at intervals of 0.5, 1, 2, 4, 6, 8, 12, 16, and 24 h and the aliquots were replenished with same volume of PBS buffer at every time interval. To investigate the absorbance of the processed samples, UV-spectrophotometer scanning was employed. Below mentioned formula was introduced to calculate the drug concentrations at various time intervals and %cumulative drug release (%CDR):

$$\%CDR = Conc. \times DF \times Vol.ofReleaseMedia \div Amt.ofdrugadded \times 100$$

Where Conc. = concentration of the drug, DF = Dilution Factor.

The various kinetic models such as Korsmeyer-Peppas, Higuchi, Zero-order and First-order model were processed to study the drug release results from the SXE-Ns-Opt (Gupta et al., 2020). To select the best model, criteria was set as drug release nearer to 1 ($R^2$) will be declared as best suited.

*2.2.11. Confocal laser scanning microscopy*

The confocal laser scanning microscopy (CLSM) was used to detect the depth of penetration of rat's intestine induced with the rhodamine loaded SXE-Ns-Opt and rhodamine red B dye solution. The rat's intestines with rhodamine red B dye solution as control and with the rhodamine loaded SXE-Ns-Opt were prepared into slices to prepare microscopic slides. CLSM was used to measure the niosomes' depth of penetration. The Argon laser beam produced optical excitation of rhodamine red dye at 514 nm, and fluorescence emission was analyzed beyond 532 nm (Pandit et al., 2021).

*2.2.12. Antioxidant study*

DPPH reagent methodology was implemented to investigate the antioxidant potential of prepared formulation. The SXE and SXE-Ns-Opt were dissolved in methanol individually and further provided with 0.4 mM solution of DPPH (0.4 mL) which was incubated for one hour in obscure condition. The fulfillment of the reaction after one hour of incubation was observed by the dissipation of violet color DPPH solution due to oxidization of antioxidants. The control solution was formulated by adding the sample and DPPH solution. Further blank solution was prepared by adding methanol and DPPH. The samples quantification was estimated by UV–visible spectrophotometer at 517 nm (Baliyan et al., 2022).

*2.2.13. α-amylase inhibition assay*

The antidiabetic activity of SXE and SXE-Ns-Opt was investigated using α-amylase inhibition assay in a controlled *in-vitro* study (Khan et al., 2022). Concentrations ranging from 50 to 500 μg/mL for SXE and SXE-Ns-Opt were concocted by infusing 500 μL of sodium phosphate buffer (0.02 M) with sodium chloride (6 mM) into the sample solutions incubated at 37 °C for 20 min.

**Table 2**
Composition and optimization of PZE-Ns.

| Formulation codes | *Independent variables* | | | *Dependent variables* | | |
|---|---|---|---|---|---|---|
| | **Cholesterol (mg)** | **Span 20 (mg)** | **Sonication time (min)** | **Vesicles size (nm)** | **PDI** | **Entrapment efficiency (%)** |
| SXE-Ns-1 | 100 | 70 | 2.5 | 285 | 0.251 | 73.1 |
| SXE-Ns-2 | 100 | 70 | 2.5 | 285.2 | 0.252 | 73.2 |
| SXE-Ns-3 | 100 | 80 | 2 | 246.9 | 0.235 | 69 |
| SXE-Ns-4 | 80 | 70 | 2 | 271.2 | 0.161 | 68.3 |
| SXE-Ns-5 | 120 | 80 | 2.5 | 273.7 | 0.295 | 76.3 |
| SXE-Ns-6 | 120 | 70 | 2 | 342.8 | 0.371 | 86.5 |
| SXE-Ns-7 | 120 | 70 | 3 | 311.1 | 0.339 | 81.2 |
| SXE-Ns-8 | 80 | 60 | 2.5 | 281.9 | 0.175 | 72.6 |
| SXE-Ns-9 | 80 | 70 | 3 | 251.2 | 0.141 | 63.1 |
| SXE-Ns-10 | 100 | 60 | 3 | 294.6 | 0.281 | 78.2 |
| SXE-Ns-11 | 100 | 70 | 2.5 | 285.4 | 0.253 | 73.2 |
| SXE-Ns-12 | 100 | 80 | 3 | 214.6 | 0.219 | 65.1 |
| SXE-Ns-13 | 120 | 60 | 2.5 | 372.2 | 0.392 | 91.1 |
| SXE-Ns-14 | 100 | 60 | 2 | 315.1 | 0.319 | 84.9 |
| SXE-Ns-15 | 80 | 80 | 2.5 | 229.8 | 0.115 | 57.9 |

Further, one percent starch was prepared with sodium phosphate buffer (0.02 M) from which 250 µL was added to the reaction mixture and incubated for 10 min. To cease the reaction, 1 mL of dinitrosalicylic acid was incorporated and accompanied by incubation in water bath at 100 °C for 15 min. After subsiding the heat from reaction mixture incubated at room temperature, the absorbance was observed at 540 nm. The reaction mixtures without niosomes and with acarbose at different concentrations (50 to 500 µg/mL) were used to observe absorbance. To calculate the percentage of inhibition of α-amylase formula used was as:

$$Percentageofinhibition = [(Ac - As)/Ac] \times 100$$

Where, Ac = absorbance of control
As = absorbance of sample.

*2.2.14. α-glucosidase inhibition assay*

The α-glucosidase inhibition assay was modification of the method previously described (Dou et al., 2019). SXE and SXE-Ns-Opt with various concentrations were mixed with freshly prepared 0.1 mol/L potassium phosphate buffer (pH 6.9) made up to total volume of 150 µL and further homogenized to concentration from 50 to 500 µg/mL. 10 µL of α-glucosidase solution (1 unit/mL/min) (Sigma-Aldrich, Inc., Darmstadt, Germany) was added. The reaction mixer was kept under controlled environment at 37 °C for 15 min. Then, 3 mM p-nitrophenyl-α-Dglucopyranoside (PNP-G) was prepared and 10 µL of it was added. The mixture was re-incubated at room temperature for 10 min. The addition 0.1 M $Na_2CO_3$was used to cease the reaction. The UV spectrophotometer at 405 nm was used to assess the enzymatic activity of the amount liberated byproduct (p-nitrophenol). α-glucosidase inhibitor i.e. acarbose was used as a positive control. The absorbance was measured in triplicate. The below mentioned formula was used to calculate the percentage of inhibition:

$$\%Inhibitionactivity = [(Acontrol - Asample)/Acontrol] \times 100$$

Where A is the absorbance measured at 405 nm.

*2.2.15. Stability study*

The prepared SXE-Ns-Opt samples were covered in aluminum-sealed glass containers and stored at 2 to 8 °C (refrigerator) for the duration of 60 days. Samples were withdrawn at 0, 30 & 60 days and evaluated for vesicles size and EE% (Nakhaei et al., 2021).

## 3. Results

### 3.1. Total phenolic and flavonoid content

Polyphenols are beneficial plant compounds which have been found to be with powerful antioxidants property that prevent or reverse damage in cells caused by various factors. The TPC and TFC of SXE were shown in Fig. 1. The preferable results showed the abundant level of TPC and TFC in SXE as 188.92 GA Eq/g and 142.40 Q Eq/g respectively.

### 3.2. Niosome optimization employing the Box-Behnken design

For the development of formulation, 15 experimental runs were generated by the Box–Behnken design with three center points (Table 1). Three dependent variables namely vesicle size, PDI and entrapment efficiency were in the range of 214.6 nm to 372.2 nm, 0.115 and 0.392 and 57.9 to 91.1%, respectively. For the 15 formulations, it was discovered that the quadratic model is the most suitable model. In Table3, the $R^2$, SD, and %CV values for each of the three responses are displayed. The three-dimensional graph (Figs. 2, 3 and 4) shows the influence of independent factors on the size of vesicle, PDI and entrapment efficiency and quantitatively compares the experimentally obtained responses to those were predicted.

*3.2.1. Independent variables impact on vesicle size*

Cholesterol was found to be having a positive effect on vesicle size and span 20 to be having a negative effect as shown in equation below.

$$Y = +285.20 + 33.21X1 - 37.35X2 - 13.06X3 - 11.60X1 \times X2 - 2.93X1 \times X3 - 2.95X2 \times X3 + 15.24X1^2 - 11.04X2^2 - 6.36X3^2$$

Overall 15 experimental runs mean vesicle size was determined to be 284.05 nm, with data that varied from lowest to highest of 214.6 nm to 372.2 nm, respectively. It was shown that as cholesterol levels increased, the size of niosome vesicles increased. It was observed that vesicles size was increased from 229.8 nm (formulation 15) to 342.8 nm (formulation 6) when ratio of cholestrol was enhanced from 80 mg (formulation 15) to 120 mg (formulation 6). Comparable outcomes were obtained with formulation 9 (251.2 nm) and formulation 13 (vesicles size 372.2 nm) Table 2 and Fig. 2. Table 2 makes evident the impact of span 20. It was found that span 20 had an opposite effect on the size of the vesi-

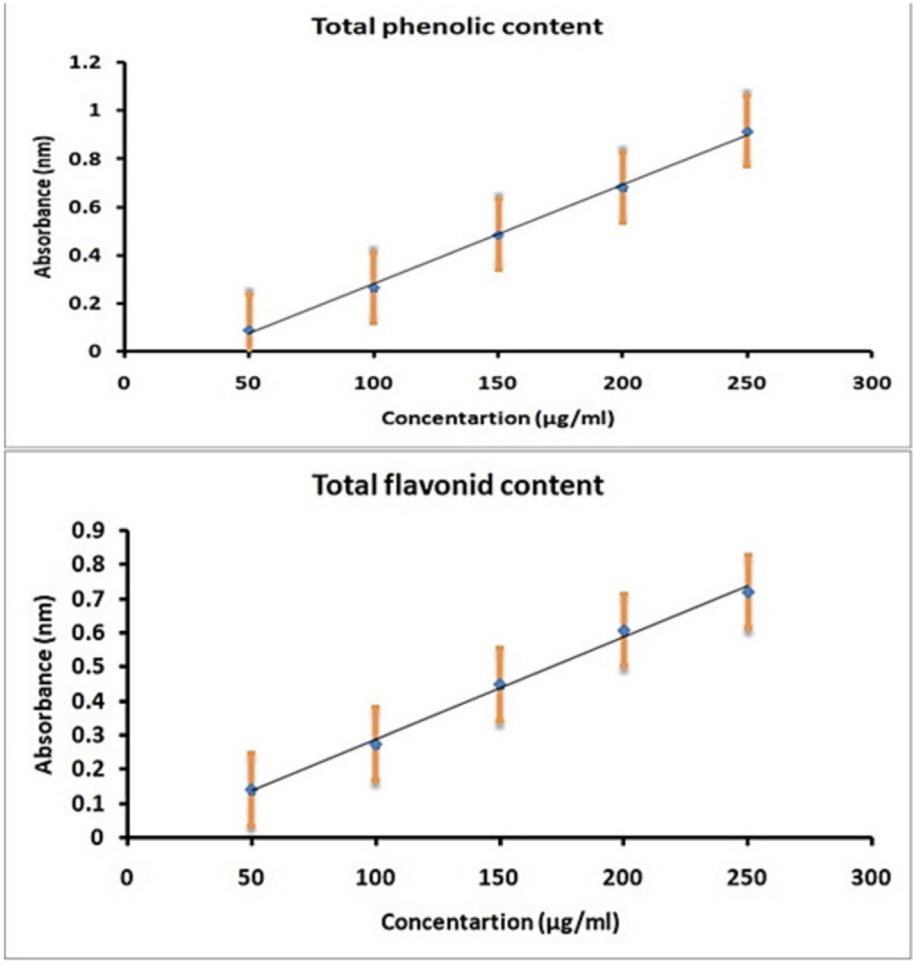


**Fig. 1.** Total phenolic content and total flavonoid content of *S. xanthocarpum* ethanolic extract.

**Table 3**
Summary of results of regression analysis for responses Y1, Y2 and Y3 for fitting to the quadratic model.

| Quadratic model | $R^2$ | Adjusted $R^2$ | Predicted $R^2$ | Std. Dev. | C.V.% | Adequate precision |
|---|---|---|---|---|---|---|
| Response Y1 | 0.9999 | 0.9998 | 0.9988 | 0.6103 | 0.2149 | 315.30 |
| Response Y2 | 0.9997 | 0.9990 | 0.9948 | 0.0026 | 1.01 | 132.55 |
| Response Y3 | 0.9999 | 0.9998 | 0.9989 | 0.1297 | 0.1747 | 310.80 |

cles. The synthesized niosomes vesicles size was smaller as the span 20 was increased from 60 mg to 80 mg. Formulation 14 with 60 mg of span 20 displayed vesicles measuring from 351.1 nm, while Formulation 3 with 80 mg of span 20 had vesicles measuring from 246.9 nm. Similarly, formulation 12 (span 20 80 mg) displayed vesicles with a size of 214.6 nm and formulation 8 (span 20 60 mg) displayed vesicles with a size of 281.9 nm. Sonication time also showed effects on the size of vesicle. Formulation 6 was prepared with less sonication time (2 min) than Formulation 12 (3 min), which resulted in larger vesicles. Similarly, formulation 2 with sonication time 2 min showed the vesicle size of 285.2 nm while formulation 9 with sonication time 3 min showed the vesicle size of 251.2 nm.

*3.2.2. Independent variables' impact on PDI*

Experimental results showed that the independent variable was cholesterol and had a positive effect on PDI (Fig. 3, Table 2) as can be shown by the equation below.

$$Y = +0.2520 + 0.1006X1 - 0.0379X2 - 0.0132X3 - 0.0092X1 * X2 - 0.0030X1 * X3 + 0.0055X2 * X3 - 0.0091X1^2 + 0.0014X2^2 + 0.0101X3^2$$

Cholesterol showed a substantial impact on PDI. An increase in the PDI from 0.115 (formulation 15) to 0.392 (formulation 13) was observed with increasing cholesterol concentration from 80 mg to 120 mg. The formulations 5, 6, 7 and 13 with maximum concentration of cholestrol (120 mg) showed high level of PDI. It was also observed that increasing cholestrol and sonication time and decreasing span 20 value directly improves the PDI as seen in formulation 5, 7 and 10 (Fig. 3).

*3.2.3. Independent variables' impact on entrapment efficiency*

The ratio of cholestrol had an optimistic act on the entrapment efficiency, and span 20, had a negative result on the drug entrapment efficiency which can be shown by the equation mentioned below.

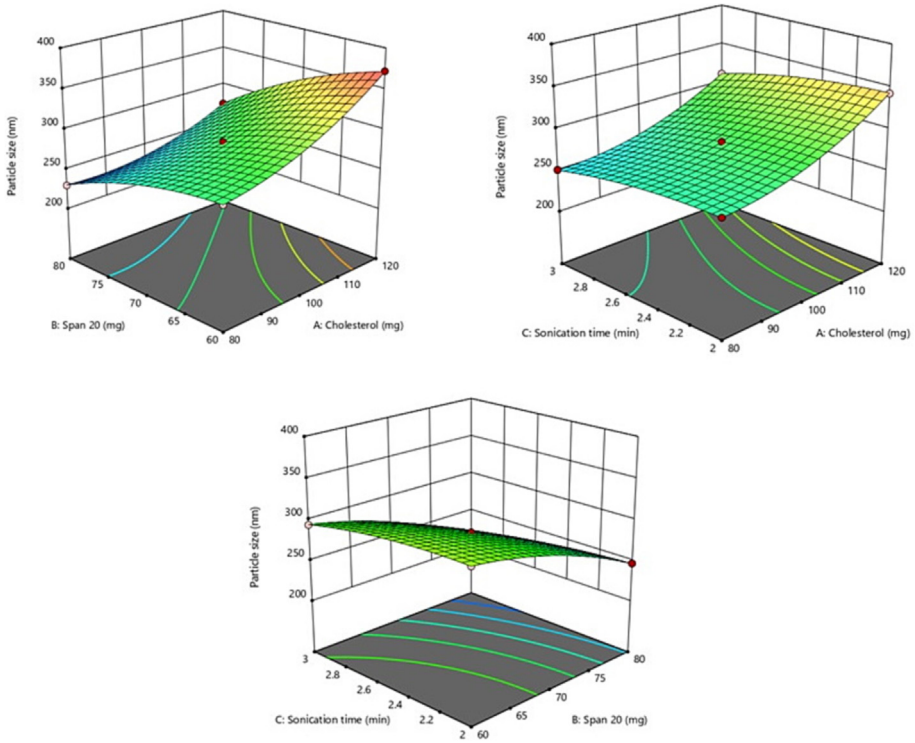


**Fig. 2.** 3D response surface plot showing effect of independent variables on vesicles size.

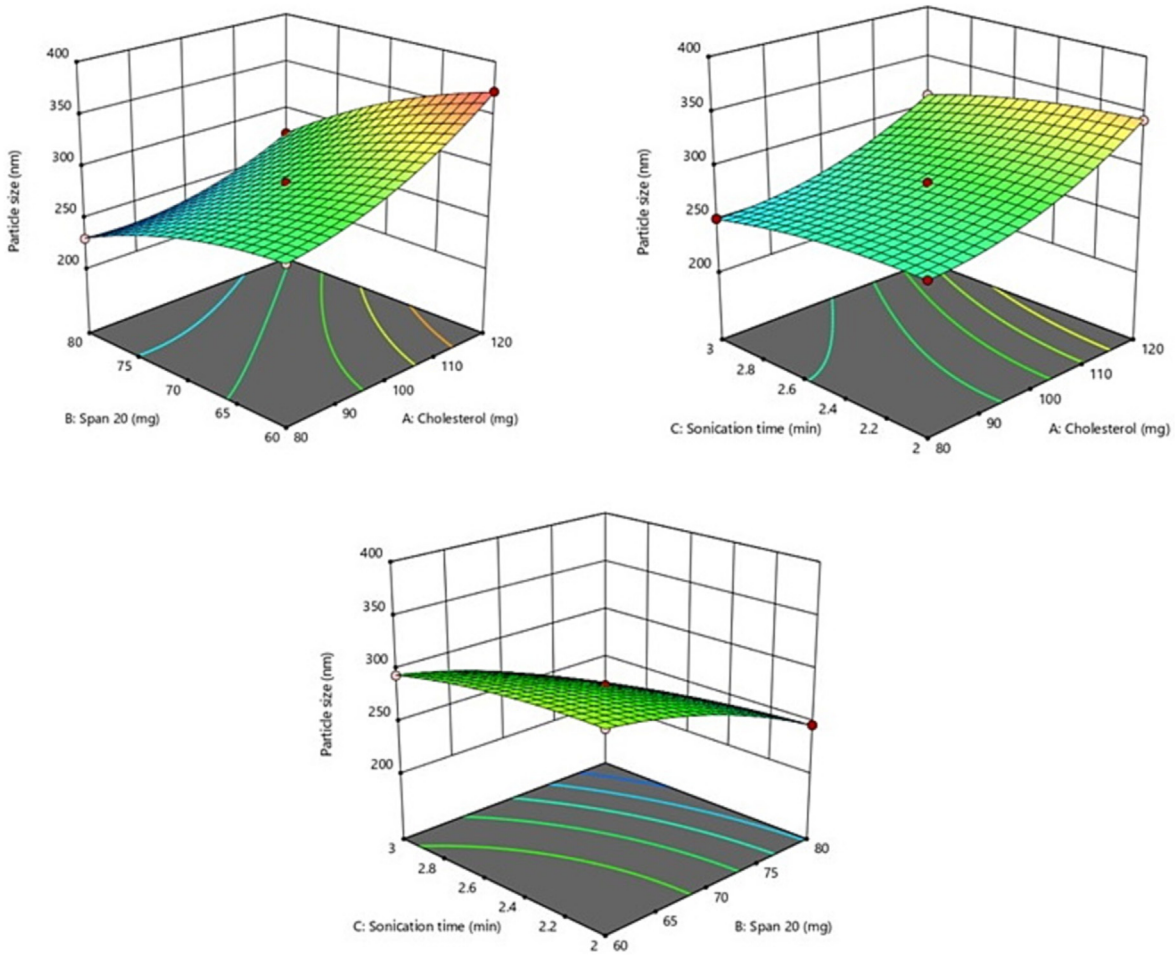


**Fig. 3.** 3D response surface plot showing effect of independent variables on PDI.

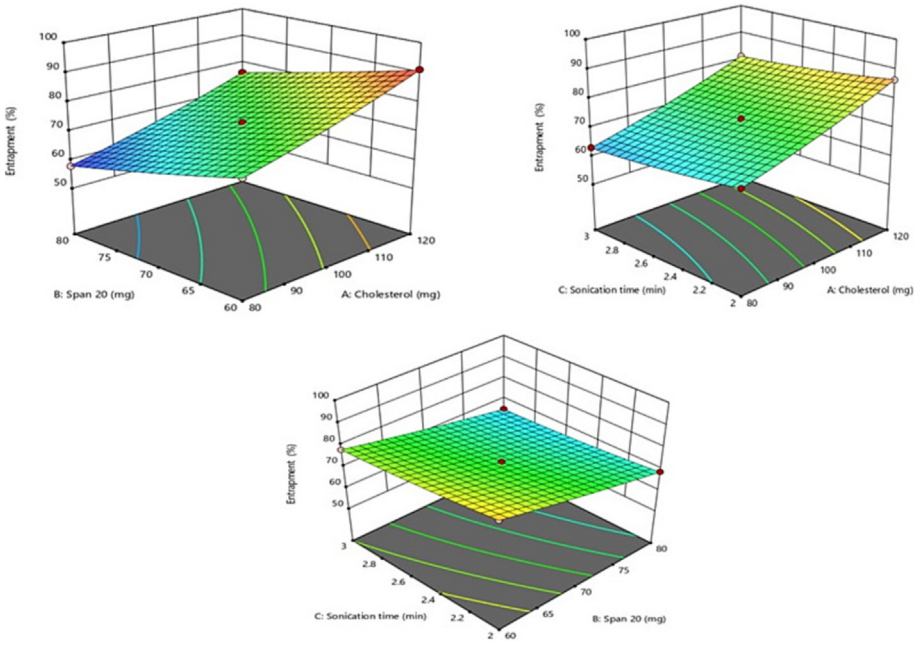


**Fig. 4.** 3D response surface plot showing effect of independent variables on EE%.

$$Y = +73.17 + 9.15X1 - 7.31X2 - 2.64X3 - 0.0250X1 * X2 - 0.0250X1 * X3 + 0.7000X2 * X3 + 0.8917X1^2 + 0.4167X2^2 + 0.7167X3^2$$

The entrapment efficiencies for all formulations ranged between the lower and higher values of 57.9% and 91.1%, with an average value of 74.24% (Table 2). In contrast to the formulation 15 that contained 80 mg of cholestrol and displayed an entrapment efficiency of 57.9%, formulation 13 (120 mg) had an entrapment efficiency of 91.1%. Similar outcomes were seen between formulation 2 (73.2%) and formulation 9 (63.1%). For formulations 6 and 10, similar outcomes were obtained (Table). Span20 had a negative impact on the effectiveness of the entrapment of *S. xanthocarpum* extract in niosomes. Formulation 8 (span 20, 60 mg) presented entrapment efficiency of 72.6% while the formulation 3 (span 20 80 mg) presented entrapment efficiency of 69%. Formulation 9 (span 20, 70 mg) presented entrapment efficiency 63.1% and formulation 12 (span 20, 80 mg) presented entrapment efficacy of 65.1%. This might be because vesicles start to leak more with greater span 20. As the sonication period was increased, entrapment efficiency similarly declined. Formulation 6 (sonication time 2 min) presented entrapment efficiency of 68.3% while formulation 10 (sonication time 3 min) presented entrapment efficiency of 78.2%. Similar results were obtained between formulation 11 with sonication time 2.5 min (entrapment efficiency 73.2%) and formulation 7 with sonication time 3 min (entrapment efficiency 81.2%).

### 3.2.4. Point prediction

The point prediction method was immersed for the selection of optimized formulation and further characterization. The optimized formulation i.e. SXE-Ns-Opt composed for cholesterol (120 mg), Span 20 (80 mg), and sonication time (2.5 min). Vesicle size was actually 273.76 nm, PDI was 0.295 and entrapment efficiency was 76.3 % (Fig. 5A). The predicted values displayed size of vesicle as 282.76 nm (Fig. 5A), PDI of 0.198 and entrapment efficiency of 76.64%.

### 3.3. TEM

The micrograph of TEM confirmed the morphology and presence of SXE-Ns-Opt formulation. The micrograph revealed uniform size distribution and spherical shaped sealed structures of the optimized SXE-Ns-Opt formulation (Fig. 5B).

### 3.4. Thermal analysis

The cholesterol, span20, SXE and SXE-Ns-Opt formulation was used for DSC thermograms as illustrated in Fig. 6. The cholesterol exhibited one sharp endothermic peak at 148.969 °C as seen in Fig. 6A. Span20 showed endothermic peak at 18.479 °C as presented in Fig. 6B. SXE displayed endothermic peak at 124.918 °C as seen in Fig. 6C. The SXE-Ns-Opt mainly showed single and sharp endothermic peak at 169.479 °C as shown in Fig. 6D. As the peak of optimized formulation was found to be totally different from other excipients and extract peaks as seen in Fig. 6. So it may be concluded that of cholesterol and Span 20 combination with SXE or interaction with SXE as there was no further free SXE peak found, recommending that the drug was completely encapsulated. This confirms the SXE niosomes formation and no leakage of SXE predicted.

### 3.5. FTIR spectra

SXE and SXE-Ns-Opt formulation were compared by demonstrating the FTIR to understand the compatibility with excipients (Fig. 7). The characteristic spectrum of SXE sample exhibited peaks at 3744.96, 2927.10, 1867.17, 1617.38, 1393.63, 1254.75, 1056.07, 930.69, 774.44, and 615.32 $cm^{-1}$. The SXE-Ns-Opt demonstrated peaks at 3742.03, 2905.89, 1868.14, 1645.35, 1463.07, 1281.75, 1083.08, 929.73, 782.17, and 630.75 $cm^{-1}$. The FTIR spectra demonstrated the characteristic peaks of SXE sample that was also found in the spectra peaks of SXE-Ns-Opt, attachment can suggest a covalent bond formation of SXE molecules of optimized formulation with excipients without any changes and modification. Attachment can suggest a covalent bond formation.

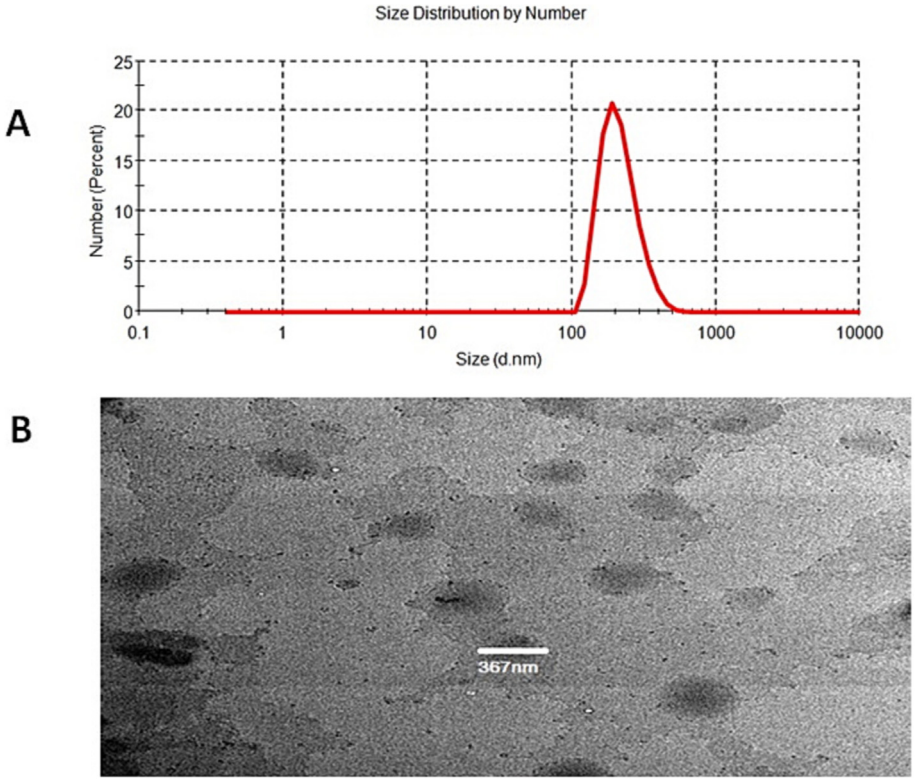


**Fig. 5.** (A) Vesicles size, and (B) TEM image of optimized formulation SXE-Ns-Opt.

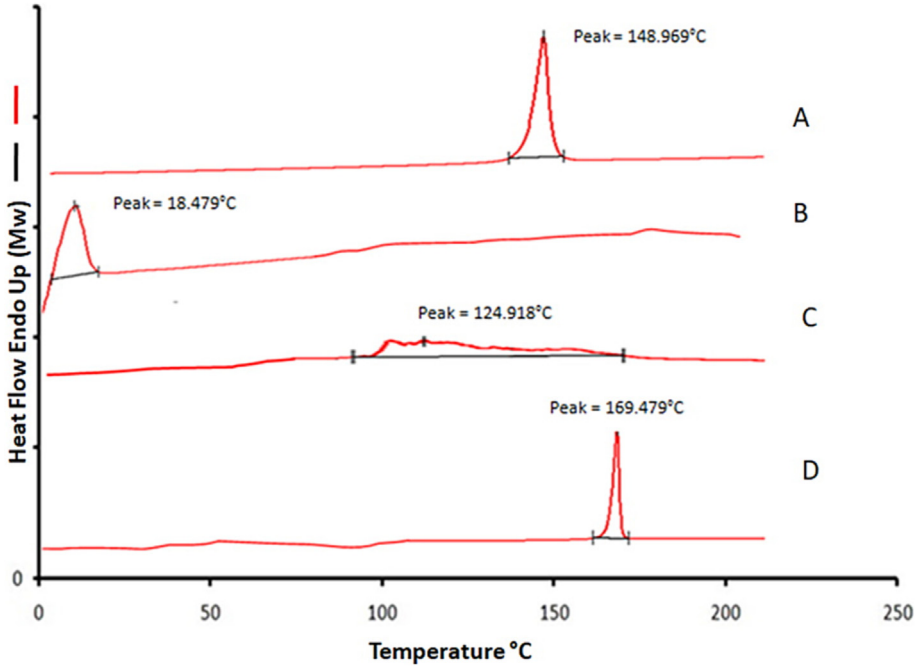


**Fig. 6.** DSC image: (A) Cholesterol, (B)Span 20, (C) SXE, and (D) SXE-Ns-Opt.

### *3.6. In-vitro drug release*

In order to assess the release behavior, SXE-Ns-Opt and SXE suspension were compared by performing *in-vitro* drug release study as shown in Fig. 8. It was observed that SXE from SXE suspension was released rapidly within 6 h of experiment i.e. 26.6% of cumulative release and at 24 h showed release of 47.37%. While SXE-Ns-Opt showed extended drug release and initially showed a sudden release that might have been caused by the unentrapped drug. Later at 12 h SXE-Ns-Opt showed a SXE release of 79.31% and at 24 h showed 82.74%. The Fig. 8 attributed to initial few hours burst release of the SXE followed by a prolonged release up to 24 h. The fresh buffer was used to maintain the sink condition by the replenishing the receiver medium but this can't mimic the sink condition

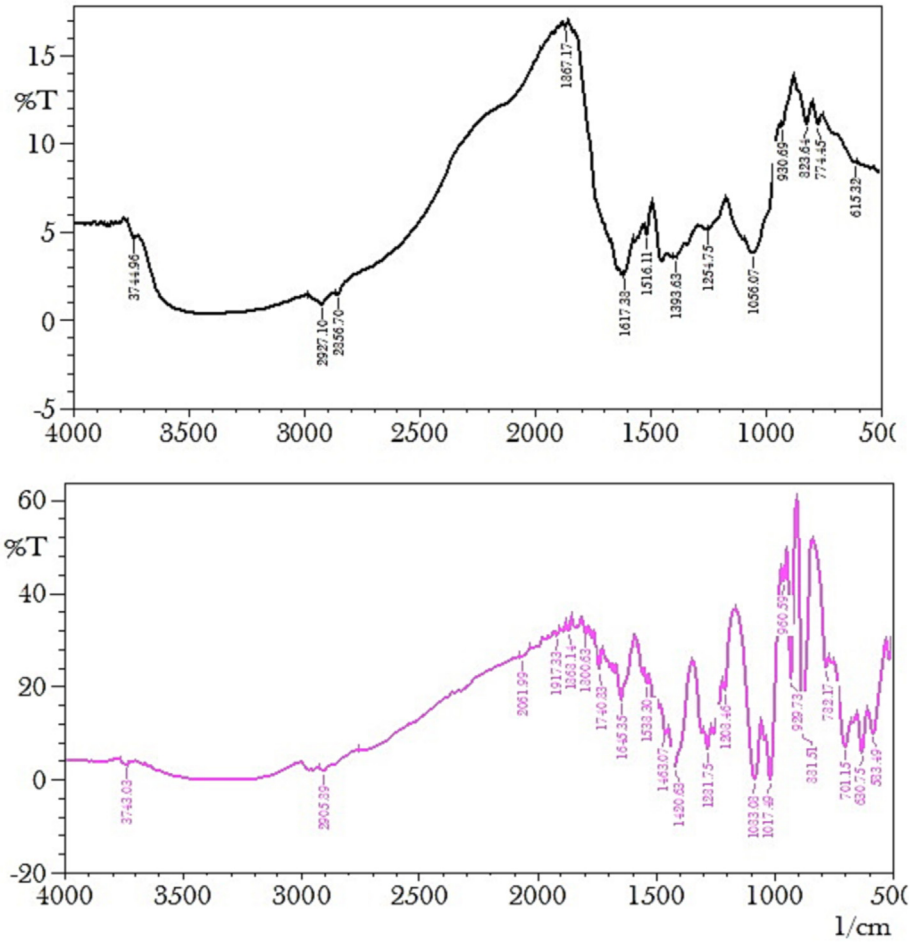


**Fig. 7.** FT-IR spectra of (A) SXE and (B) SXE-Ns-Opt.

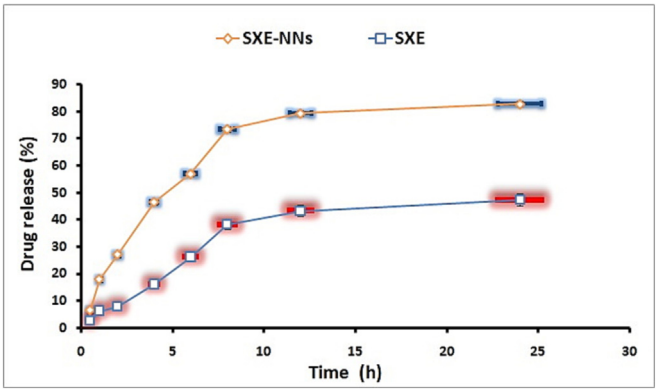


**Fig. 8.** Comparative drug release of SXE and SXE-Ns-Opt.

completely. As an outcome, it could fail to be possible to eliminate entire drugs from the matrix.

To analyze the drug release data, a variety of drug release kinetic models, including the Korsmeyer-Peppas, Higuchi, Zero-order, and First-order models, were used. The fitting model showed release mechanism as least by Korsmeyer-Peppas model presented highest $R^2$ = 0.918 value, Higuchi model gave value of $R^2$ = 0.873, First order value of $R^2$ = 0.805 and least fitting showed by Zero order $R^2$ = 0.682. Hence, Korsmeyer-Peppas model exhibited as a best fit model for the release of SXE from SXE-NS-Opt.

### 3.7. Confocal laser scanning microscopy (CLSM)

Photomicrographs of CLSM analysis showed that dye rhodamine B solution penetration Fig. 9A indicating that the only the topmost layers continued to be restricted to suspension of rat's intestine and penetrates up to 15 µm. While SXE-Ns-Opt loaded with rhodamine dye solution showed high fluorescence intensity throughout the various layers of intestine and depicted permeation up to 30 µm depth (Fig. 9B). The darkening of intestinal layers clarifies the higher penetration. This enhanced penetration of rhodamine loaded SXE-Ns-Opt may be due to the cholesterol which lead to the extend exposure time with rat intestines.

### 3.8. Antioxidant activity

Antioxidants are the chemically synthetic or natural origins which have the ability to bind with free oxygen radicals to prevent, oppose or delay the reaction. In this study, the SXE-Ns-Opt and SXE were compared to assess the antioxidant potential by DPPH method. The standard for antioxidant study used was ascorbic acid. Ascorbic acid, SXE, and SXE-Ns-Opt showed concentration-dependent inhibitory effects on DPPH with the concentration from 20 to 150 µg/mL. The antioxidant activity of ascorbic acid, SXE-Ns-Opt, and SXE was 93.41%, 88.46% and 84.74%, respectively (Fig. 10). Hence it could be understood that the prepared SXE-Ns-Opt has high potential as compared to SXE in the treatment of various diseases associated with oxidative stress.

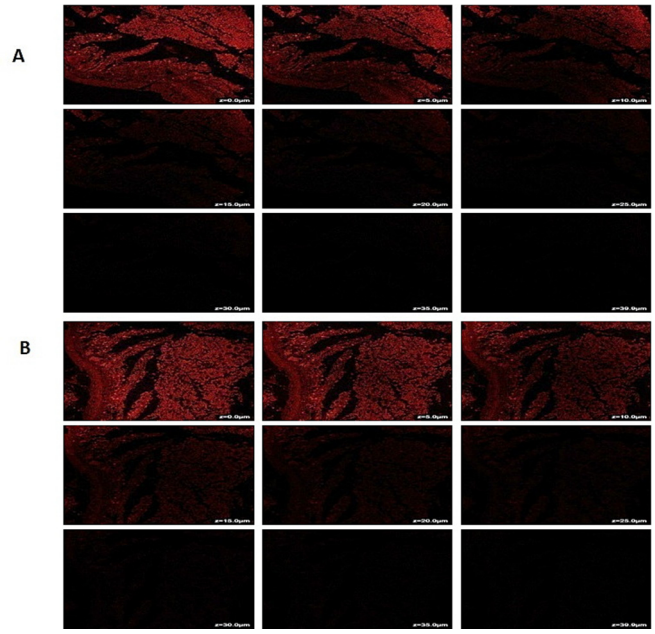


**Fig. 9.** CLSM image of rat intestine treated with (A) rhodamine red B solution, and (B) rhodamine red B loaded PZE-Ns-Opt showing depth of penetration.

### 3.9. Inhibitory assay of α-amylase and α-glucosidase assay

The key metabolizing enzymes which lead to the breakdown of glucose and enhance the absorption by GIT are *α-amylase* and *α-glucosidase*, leading to the hyperglycemia. Inhibition of these enzymes involved in breakdown of carbohydrates, leading to diminishing of blood glucose level. The inhibitory action of SXE, SXE-Ns-Opt and acarbose were shown in Fig. 11. The α-amylase was inhibited at highest level by standard (acarbose), followed by SXE-Ns-Opt and SXE as 96.07%, 92.22% and 84.64% respectively. The acarbose, SXE-Ns-Opt and SXE had a significant inhibitory effect on α-amylase with a slight better effect presented SXE ($IC_{50}$ = 84.75 μg/mL), even if the activity is comparable with SXE-Ns-Opt ($IC_{50}$ = 95.85 μg/mL). Worth of note, the extract and the formulation in niosomes showed higher inhibitory activity than acarbose ($IC_{50}$ of 130 μg/mL). The α-glucosidase inhibition assay findings revealed that acarbose demonstrated superior level of inhibition potency as 88.47%, SXE-Ns-Opt as 85.78%, and SXE as 81.07%respectively. The $IC_{50}$ value for standard drug acarbose, SXE-Ns-Opt and SXE was found to be 92.87 μg/mL, 84.89 μg/mL and 73.52 μg/mL, respectively.

### 3.10. Stability study

The stability studies of SXE-Ns-Opt formulation were performed to evaluate the stability during storage period (2 months) and any loss of drug from niosomes. At the end of first month, stored formulation SXE-Ns-Opt at refrigerator temperature (4 °C/ 60 ± 5% RH) was evaluated for EE% and vesicles size. The results recorded EE% and vesicles size as 67.6 ± 5.5% and 270.33 ± 8.5 nm as mentioned in Table 4. After 60 days, optimized formulation was again determined using the same method opted as that of entrapment efficiency and vesicle size. The results showed EE% and vesicles size as 61.71 ± 3.2% and 273 ± 5.2 nm and concluded to be stable under refrigerated conditions.

## 4. Discussion

Numerous claimed therapeutic effects of *S. xanthocarpum* include cardio-protection, anti-inflammation, anti-microbial, anti-fungal, antihyperglycemic, and wound healing. However, *S. xanthocarpum* extract has problems with permeability that may be associated with the size of the molecules present, their solubility, bioavailability, etc (Elizalde-Romero et al., 2021; Singh et al., 2022). It's been proven that nanosized formulations loaded with extracts have overcome their limitations including improvement in solubility, stability, bioavailability, permeation, pharmacological activity, etc (Kumari et al., 2022). However, this work is the initial in-depth study of *S. xanthocarpum* that optimizes their pharmacokinetics using a variety of niosomal preparations to improve their *ex-vivo* and *in-vitro* antidiabetic activity, and antioxidant potential. The optimized formulation, SXE-Ns-Opt, initially showed burst release but afterwards revealed the slow release of *in-vitro* drug release study, which may have been caused by the release

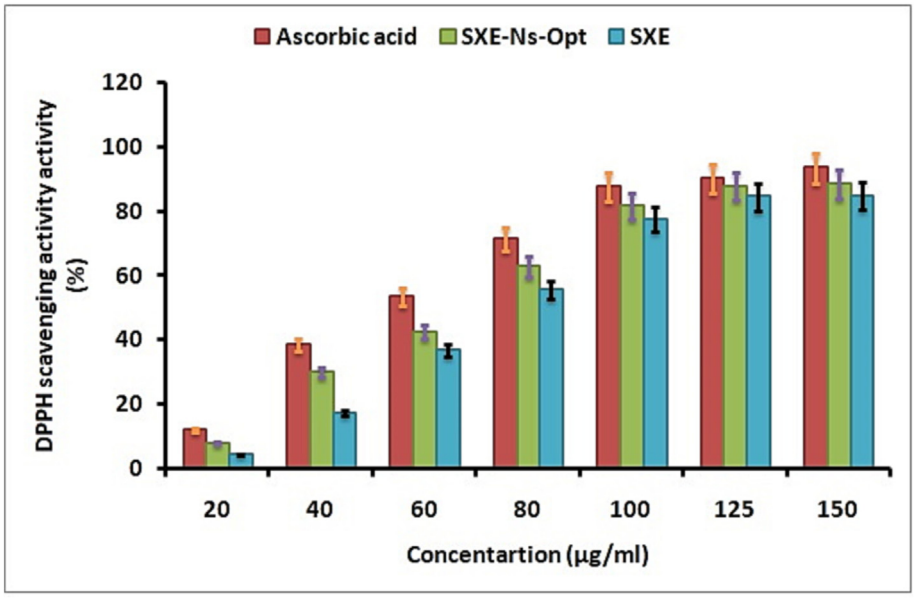


**Fig. 10.** DPPH scavenging activity of SXE and SXE-Ns-Opt.

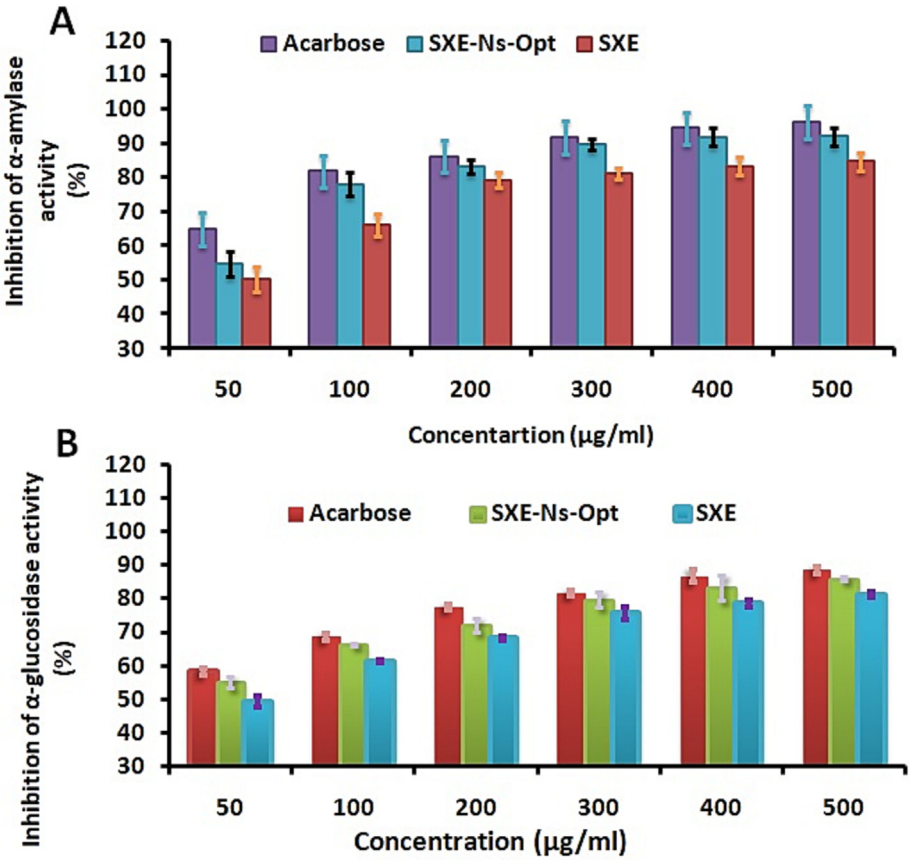


**Fig. 11.** Inhibition of (A) α-amylase, and (B) α-glucosidase activity of SXE and SXE-Ns-Opt.

**Table 4**
Stability study of SXE-Ns-Opt at 4 ± 0.5 °C.

| Observations | 0 days | 30 days | 60 days |
|---|---|---|---|
| Vesicle size | 270.33 ± 8.5 nm | 273 ± 5.2 nm | 268.66 ± 5.5 nm |
| EE% | 69.27 ± 3.8 % | 67.6 ± 5.5 % | 61.71 ± 3.2 % |

of SXE that was loosely bound to excipients and SXE which was incorporated completely in formulation released at slow pace. The models studied were Korsmeyer-Peppas, Higuchi, Zero-order, and First-order models, and best fitted model to study drug release was Korsmeyer-Peppas model. The optimized formulation displayed the vesicles with a diameter of 253.6 nm, a PDI of 0.108, an entrapment efficiency of 62.4%, and an 84.01% drug release. The CLSM study was performed to examine the penetration of optimized formulation as compared to control on rat's intestinal mucus barrier. The CLSM images showed high degree of penetration of optimized formulation which indicated the reduction in particle size was necessary to improve bioavailability and ultimately leading to the penetration through various layers of intestine. *In vitro* antidiabetic studies, α-amylase and α-glucosidase activity was performed to understand the level of inhibition of α-amylase and α-glucosidase enzymes by optimized formulation and SXE. Both the enzymes have the potential to breakdown the carbohydrates into simple absorbable carbohydrates and get absorbed through the intestine into the bloodstream. Optimized formulation presented higher impact and showed dose dependent pattern in inhibition of enzymes than SXE. The inhibition of α-amylase was recorded as 85.88% (SXE), and 89.87% (optimized formulation), and also suppressed the enzyme α-glucosidase by 81.07% (SXE), and 85.78% (optimized formulation). Additionally, the strong antioxidant potential also proved the efficiency of optimized formulation as compared to SXE, respectively 89.46% and 78.10% and might be responsible for ameliorating antidiabetic and its complications.

## 5. Conclusions

The current investigation serves to reinforce the background of *S. xanthocarpum* in diabetes and antioxidant study. According to the results of the experiment described above, the SXE-loaded niosomes were successfully synthesized by solvent evaporation method. The Box-Behnken design was processed by using cholesterol, span 20 and sonication time to optimize the formulation. Vesicle size, PDI, and EE% were chosen variables to assess for the fifteen formulations. FTIR and DSC clearly showed the complex formation of SXE and excipients. The *in-vitro* release study initially indicated the burst release and further showed the slow release. The best fitted model found as per the $R^2$ value was korsmeyer-Peppas model. The According to the CLSM investigation, the improved formulation SXE-Ns-Opt had enhanced intestinal penetration in rats than the control. Additionally, the formulation SXE-Ns-Opt (150 µg/mL) demonstrated efficient suppression of glucosidase and amylase enzyme activity in comparison to SXE. Thus, it might be offered that SXE-loaded niosomes might be a better dosage form for the distribution of SXE and might even be a better strategy for managing diabetes mellitus.

## Declaration of Competing Interest

The authors declare that they have no known competing financial interests or personal relationships that could have appeared to influence the work reported in this paper.

## Acknowledgement

The authors extend their appreciation to the Deputyship for Research and Innovation, "Ministry of Education" in Saudi Arabia for funding this research (IFKSUOR3-375-1).

## References

Abdel-Moneim, A., El-Shahawy, A., Yousef, A.I., Abd El-Twab, S.M., Elden, Z.E., Taha, M., 2020. Novel polydatin-loaded chitosan nanoparticles for safe and efficient type 2 diabetes therapy: In silico, in vitro and in vivo approaches. Int. J. Biol. Macromol. 154, 1496–1504. https://doi.org/10.1016/j.ijbiomac.2019.11.031.

Ahn, J.H., Kim, J., Rehman, N.U., Kim, H.J., Ahn, M.J., Chung, H.J., 2020. Effect of rumex acetosa extract, a herbal drug, on the absorption of fexofenadine. Pharmaceutics 12, 1–14. https://doi.org/10.3390/pharmaceutics12060547.

Baliyan, S., Mukherjee, R., Priyadarshini, A., Vibhuti, A., Gupta, A., Pandey, R.P., Chang, C.M., 2022. Determination of antioxidants by DPPH radical scavenging activity and quantitative phytochemical analysis of Ficus religiosa. Molecules 27. https://doi.org/10.3390/molecules27041326.

Bari, N.K., Fazil, M., Hassan, M.Q., Haider, M.R., Gaba, B., Narang, J.K., Baboota, S., Ali, J., 2015. Brain delivery of buspirone hydrochloride chitosan nanoparticles for the treatment of general anxiety disorder. Int. J. Biol. Macromol. 81, 49–59. https://doi.org/10.1016/j.ijbiomac.2015.07.041.

Cetin, E.O., Salmanoglu, D.S., Ozden, I., Ors-Kumoglu, G., Akar, S., Demirozer, M., Karabey, F., Kilic, K.D., Kirilmaz, L., Uyanikgil, Y., Sevimli-Gur, C., 2022. Preparation of ethanol extract of propolis loaded niosome formulation and evaluation of effects on different cancer cell lines. Nutr. Cancer 74, 265–277. https://doi.org/10.1080/01635581.2021.1876889.

Dou, Z., Chen, C., Fu, X., 2019. The effect of ultrasound irradiation on the physicochemical properties and α-glucosidase inhibitory effect of blackberry fruit polysaccharide. Food Hydrocoll. 96, 568–576. https://doi.org/10.1016/j.foodhyd.2019.06.002.

Elizalde-Romero, C.A., Montoya-Inzunza, L.A., Contreras-Angulo, L.A., Heredia, J.B., Gutiérrez-Grijalva, E.P., 2021. Solanum fruits: Phytochemicals, bioaccessibility and bioavailability, and their relationship with their health-promoting effects. Front. Nutr. 8, 1–9. https://doi.org/10.3389/fnut.2021.790582.

Gedikoğlu, A., Sökmen, M., Çivit, A., 2019. Evaluation of Thymus vulgaris and Thymbra spicata essential oils and plant extracts for chemical composition, antioxidant, and antimicrobial properties. Food Sci. Nutr. 7, 1704–1714. https://doi.org/10.1002/fsn3.1007.

Ghasemian, E., Vatanara, A., Navidi, N., Rouini, M.R., 2017. Brain delivery of baclofen as a hydrophilic drug by nanolipid carriers: Characteristics and pharmacokinetics evaluation. J. Drug Deliv. Sci. Technol. 37, 67. https://doi.org/10.1016/j.jddst.2016.06.012.

Gudise, V., Chowdhury, B., Manjappa, A.S., 2021. Antidiabetic and antihyperlipidemic effects of Argyreia pierreana and Matelea denticulata: Higher activity of the micellar nanoformulation over the crude extract. J. Tradit. Complement. Med. 11, 259–267. https://doi.org/10.1016/j.jtcme.2020.08.001.

Gupta, D.K., Aqil, M., Ahad, A., Imam, S.S., Waheed, A., Qadir, A., Iqubal, M.K., Sultana, Y., 2020. Tailoring of berberine loaded transniosomes for the management of skin cancer in mice. J. Drug Deliv. Sci. Technol. 60. https://doi.org/10.1016/j.jddst.2020.102051.

Hsueh, T.P., Lin, W.L., Tsai, T.H., 2017. Pharmacokinetic interactions of herbal medicines for the treatment of chronic hepatitis. J. Food Drug Anal. 25, 209–218. https://doi.org/10.1016/j.jfda.2016.11.010.

Jeevanandam, J., Chan, Y.S., Danquah, M.K., 2016. Nano-formulations of drugs: Recent developments, impact and challenges. Biochimie 128–129, 99–112. https://doi.org/10.1016/j.biochi.2016.07.008.

Jin, Y., Wen, J., Garg, S., Liu, D., Zhou, Y., Teng, L., Zhang, W., 2013. Development of a novel niosomal system for oral delivery of Ginkgo biloba extract. Int. J. Nanomed. 8, 421–430. https://doi.org/10.2147/IJN.S37984.

Joghee, S., 2019. Solanum xanthocarpum: A review. Int. J. Pharmacogn. Chinese Med. 3, 1–7. https://doi.org/10.23880/ipcm-16000177.

Khan, B.A., Hamdani, S.S., Ahmed, M.N., Hameed, S., Ashfaq, M., Shawky, A.M., Ibrahim, M.A.A., Sidhom, P.A., 2022. Synthesis, X-ray diffraction analysis, quantum chemical studies and α-amylase inhibition of probenecid derived S-alkylphthalimide-oxadiazole-benzenesulfonamide hybrids. J. Enzyme Inhib. Med. Chem. 37, 1464–1478. https://doi.org/10.1080/14756366.2022.2078969.

Kumar, S., Baldi, A., Sharma, D.K., 2021. In vitro antioxidant assay guided ex vivo investigation of cytotoxic effect of phytosomes assimilating taxifolin rich fraction of Cedrus deodara bark extract on human breast cancer cell lines (MCF7). J. Drug Deliv. Sci. Technol. 63, 102486. https://doi.org/10.1016/j.jddst.2021.102486.

Kumari, S., Goyal, A., Gürer, E.S., Yapar, E.A., Garg, M., Sood, M., Sindhu, R.K., 2022. Bioactive loaded novel nano-formulations for targeted drug delivery and their therapeutic potential. Pharmaceutics 14. https://doi.org/10.3390/pharmaceutics14051091.

Nakhaei, P., Margiana, R., Bokov, D.O., Abdelbasset, W.K., Jadidi Kouhbanani, M.A., Varma, R.S., Marofi, F., Jarahian, M., Beheshtkhoo, N., Pradeepa, Udaya Bhat, K., Vidya, S.M., 2021. Liposomes: Structure, Biomedical Applications, and Stability Parameters With Emphasis on Cholesterol. J. Drug Deliv. Sci. Technol. 9, 1–23. https://doi.org/10.1016/j.jddst.2016.11.002.

Padhi, S., Nayak, A.K., Behera, A., 2020. Type II diabetes mellitus: a review on recent drug based therapeutics. Biomed. Pharmacother. 131. https://doi.org/10.1016/j.biopha.2020.110708.

Pandit, J., Sultana, Y., Aqil, M., 2021. Chitosan coated nanoparticles for efficient delivery of bevacizumab in the posterior ocular tissues via subconjunctival administration. Carbohydr. Polym. 267, 118217. https://doi.org/10.1016/j.carbpol.2021.118217.

Parmar, S., Amit Gangwal, N.S.D., 2011. *** Scholars *** Scholars Research Library ***. Sch. Res. Libr. 2, 373–383.

Poongothai, K., Ponmurugan, P., Ahmed, K.S.Z., Kumar, B.S., Sheriff, S.A., 2011. Antihyperglycemic and antioxidant effects of Solanum xanthocarpum leaves (field grown & in vitro raised) extracts on alloxan induced diabetic rats. Asian Pac. J. Trop. Med. 4, 778–785. https://doi.org/10.1016/S1995-7645(11)60193-4.

Pradeepa, Udaya Bhat, K., Vidya, S.M., 2017. Nisin gold nanoparticles assemble as potent antimicrobial agent against Enterococcus faecalis and Staphylococcus aureus clinical isolates. J. Drug Deliv. Sci. Technol. 37, 20–27. https://doi.org/10.1016/j.jddst.2016.11.002.

Pungle, R., Nile, S.H., Kharat, A.S., 2023. Green synthesis and characterization of Solanum xanthocarpum capped silver nanoparticles and its antimicrobial effect on multidrug-resistant bacterial (MDR) isolates. Chem. Biol. Drug Des. 101, 469–478. https://doi.org/10.1111/cbdd.13945.

Raafat, K.M., El-Zahaby, S.A., 2020. Niosomes of active Fumaria officinalis phytochemicals: Antidiabetic, antineuropathic, anti-inflammatory, and possible mechanisms of action. Chinese Med. (United Kingdom) 15, 1–22. https://doi.org/10.1186/s13020-020-00321-1.

Rani, R., Dahiya, S., Dhingra, D., Dilbaghi, N., Kim, K.H., Kumar, S., 2017. Evaluation of anti-diabetic activity of glycyrrhizin-loaded nanoparticles in nicotinamide-streptozotocin-induced diabetic rats. Eur. J. Pharm. Sci. 106, 220–230. https://doi.org/10.1016/j.ejps.2017.05.068.

Singh, R.K., Garg, A., Shrimali, K., Jain, V., Sinha, S.K., Pradhan, J., 2022. A brief review on Solanum xanthocarpum along with phytochemical and pharmacological profile. Adv. Pharm. J., 23–31 https://doi.org/10.31024/apj.2022.7.1.3.

Song, J.W., Liu, Y.S., Guo, Y.R., Zhong, W.X., Guo, Y.P., Guo, L., 2022. Nano-liposomes double loaded with curcumin and tetrandrine: Preparation, characterization, hepatotoxicity and anti-tumor effects. Int. J. Mol. Sci. 23. https://doi.org/10.3390/ijms23126858.

Wang, R., Zhu, X., Wang, Qing, Li, X., Wang, E., Zhao, Q., Wang, Qianqian, Cao, H., 2020. The anti-tumor effect of taxifolin on lung cancer via suppressing stemness and epithelial-mesenchymal transition in vitro and oncogenesis in nude mice. Ann. Transl. Med. 8, 590–590. https://doi.org/10.21037/atm-20-3329.

Wickramasinghe, A.S.D., Kalansuriya, P., Attanayake, A.P., 2022. Nanoformulation of plant-based natural products for type 2 diabetes mellitus: From formulation design to therapeutic applications. Curr. Ther. Res. - Clin. Exp. 96. https://doi.org/10.1016/j.curtheres.2022.100672.

Yang, X., 2019. Design and optimization of crocetin loaded PLGA nanoparticles against diabetic nephropathy via suppression of inflammatory biomarkers: a formulation approach to preclinical study. Drug Deliv. 26, 849–859. https://doi.org/10.1080/10717544.2019.1642417.

Zhang, P., Wang, P., Yan, L., Liu, L., 2018. Synthesis of gold nanoparticles with Solanum xanthocarpum extract and their in vitro anticancer potential on nasopharyngeal carcinoma cells. Int. J. Nanomed. 13, 7047–7059. https://doi.org/10.2147/IJN.S180138.